Biomedical Optics EXPRESS

Rhodamine B as an optical thermometer in cells focally exposed to infrared laser light or nanosecond pulsed electric fields

David Moreau,[1,*] Claire Lefort,[1] Ryan Burke,[1] Philippe Leveque,[1] and Rodney P. O'Connor[1]

[1]*Univ. Limoges, CNRS, XLIM, UMR 7252, F-87000 Limoges, France*
[*]*david.moreau@xlim.fr*

Abstract: The temperature-dependent fluorescence property of Rhodamine B was used to measure changes in temperature at the cellular level induced by either infrared laser light exposure or high intensity, ultrashort pulsed electric fields. The thermal impact of these stimuli were demonstrated at the cellular level in time and contrasted with the change in temperature observed in the extracellular bath. The method takes advantage of the temperature sensitivity of the fluorescent dye Rhodamine B which has a quantum yield linearly dependent on temperature. The thermal effects of different temporal pulse applications of infrared laser light exposure and of nanosecond pulsed electric fields were investigated. The temperature increase due to the application of nanosecond pulsed electric fields was demonstrated at the cellular level.

OCIS codes: (170.2520) Fluorescence microscopy; (280.6780) Temperature; (260.3060) Infrared.

References and links

1. E. E. Hoover and J. A. Squier, "Advances in multiphoton microscopy technology," Nat. Photonics **7**(2), 93–101 (2013).
2. B.-H. Li, S.-S. Xie, Z. Huang, and B. C. Wilson, "Advances in photodynamic therapy dosimetry," Prog. Biochem. Biophys. **36**(6), 676–683 (2009).
3. C.-P. Richter and X. Tan, "Photons and neurons," Hear. Res. **311**, 72–88 (2014).
4. J.-M. Bec, E. S. Albert, I. Marc, G. Desmadryl, C. Travo, A. Muller, C. Chabbert, F. Bardin, and M. Dumas, "Characteristics of laser stimulation by near infrared pulses of retinal and vestibular primary neurons," Lasers Surg. Med. **44**(9), 736–745 (2012).
5. A. J. Welch, "The thermal response of laser irradiated tissues," IEEE J. Quantum Electron. **20**(12), 1471–1481 (1984).
6. E. S. Albert, J. M. Bec, G. Desmadryl, K. Chekroud, C. Travo, S. Gaboyard, F. Bardin, I. Marc, M. Dumas, G. Lenaers, C. Hamel, A. Muller, and C. Chabbert, "TRPV4 channels mediate the infrared laser-evoked response in sensory neurons," J. Neurophysiol. **107**(12), 3227–3234 (2012).
7. M. G. Shapiro, K. Homma, S. Villarreal, C.-P. Richter, and F. Bezanilla, "Infrared light excites cells by changing their electrical capacitance," Nat. Commun. **3**, 736 (2012).
8. R. Liljemalm, T. Nyberg, and H. von Holst, "Heating during infrared neural stimulation," Lasers Surg. Med. **45**(7), 469–481 (2013).
9. R. P. Joshi, A. Mishra, J. Song, A. G. Pakhomov, and K. H. Schoenbach, "Simulation studies of ultrashort, high-intensity electric pulse induced action potential block in whole-animal nerves," IEEE Trans. Biomed. Eng. **55**(4), 1391–1398 (2008).
10. X. H. Chen, S. J. Beebe, and S. S. Zheng, "Tumor ablation with nanosecond pulsed electric fields," HBPD INT **11**(2), 122–124 (2012).
11. A. G. Pakhomov, J. F. Kolb, J. A. White, R. P. Joshi, S. Xiao, and K. H. Schoenbach, "Long-lasting plasma membrane permeabilization in mammalian cells by nanosecond pulsed electric field (nsPEF)," Bioelectromagn. **28**(8), 655–663 (2007).
12. P. T. Vernier, Y. Sun, and M. A. Gundersen, "Nanoelectropulse-driven membrane perturbation and small molecule permeabilization," BMC Cell Biol. **7**(1), 37 (2006).
13. J. Song, R. P. Joshi, and K. H. Schoenbach, "Synergistic effects of local temperature enhancements on cellular responses in the context of high-intensity, ultrashort electric pulses," Med. Biol. Eng. Comput. **49**(6), 713–718 (2011).

#247362 Received 6 Aug 2015; revised 19 Sep 2015; accepted 22 Sep 2015; published 24 Sep 2015

14. G. Baffou, H. Rigneault, D. Marguet, and L. Jullien, "A critique of methods for temperature imaging in single cells," Nat. Methods **11**(9), 899–901 (2014).
15. L. Shang, F. Stockmar, N. Azadfar, and G. U. Nienhaus, "Intracellular Thermometry by Using Fluorescent Gold Nanoclusters," Angew. Chem. Int. Ed. Engl. **52**(42), 11154–11157 (2013).
16. J. S. Donner, S. A. Thompson, M. P. Kreuzer, G. Baffou, and R. Quidant, "Mapping Intracellular Temperature Using Green Fluorescent Protein," Nano Lett. **12**(4), 2107–2111 (2012).
17. L. M. Maestro, E. M. Rodríguez, F. S. Rodríguez, M. C. la Cruz, A. Juarranz, R. Naccache, F. Vetrone, D. Jaque, J. A. Capobianco, and J. G. Solé, "CdSe Quantum Dots for Two-Photon Fluorescence Thermal Imaging," Nano Lett. **10**(12), 5109–5115 (2010).
18. O. Zohar, M. Ikeda, H. Shinagawa, H. Inoue, H. Nakamura, D. Elbaum, D. L. Alkon, and T. Yoshioka, "Thermal imaging of receptor-activated heat production in single cells," Biophys. J. **74**(1), 82–89 (1998).
19. F. Vetrone, R. Naccache, A. Zamarrón, A. Juarranz de la Fuente, F. Sanz-Rodríguez, L. Martinez Maestro, E. Martín Rodriguez, D. Jaque, J. García Solé, and J. A. Capobianco, "Temperature sensing using fluorescent nanothermometers," ACS Nano **4**(6), 3254–3258 (2010).
20. L. Yang, H.-S. Peng, H. Ding, F.-T. You, L.-L. Hou, and F. Teng, "Luminescent Ru(bpy)3 2+-doped silica nanoparticles for imaging of intracellular temperature," Mikrochim. Acta **181**(7–8), 743–749 (2013).
21. J. Ferguson and A. W. H. Mau, "Spontaneous and stimulated emission from dyes. Spectroscopy of the neutral molecules of acridine orange, proflavine, and rhodamine B," Aust. J. Chem. **26**(8), 1617–1624 (1973).
22. R. F. Kubin and A. N. Fletcher, "Fluorescence quantum yields of some rhodamine dyes," J. Lumin. **27**(4), 455–462 (1982).
23. J. J. Shah, M. Gaitan, and J. Geist, "Generalized temperature measurement equations for Rhodamine B dye solution and its application to microfluidics," Anal. Chem. **81**(19), 8260–8263 (2009).
24. U. Seger-Sauli, M. Panayiotou, S. Schnydrig, M. Jordan, and P. Renaud, "Temperature measurements in microfluidic systems: heat dissipation of negative dielectrophoresis barriers," Electrophoresis **26**(11), 2239–2246 (2005).
25. J. J. Shah, S. G. Sundaresan, J. Geist, D. R. Reyes, J. C. Booth, M. V. Rao, and M. Gaitan, "Microwave dielectric heating of fluids in an integrated microfluidic device," J. Micromech. Microeng. **17**(11), 2224 (2007).
26. L. Gui and C. L. Ren, "Temperature measurement in microfluidic chips using photobleaching of a fluorescent thin film," Appl. Phys. Lett. **92**(2), 024102 (2008).
27. D. Ross, M. Gaitan, and L. E. Locascio, "Temperature measurement in microfluidic systems using a temperature-dependent fluorescent dye," Anal. Chem. **73**(17), 4117–4123 (2001).
28. P. Löw, B. Kim, N. Takama, and C. Bergaud, "High-Spatial-Resolution Surface-Temperature Mapping Using Fluorescent Thermometry," Small **4**(7), 908–914 (2008).
29. J. Sakakibara and R. J. Adrian, "Whole field measurement of temperature in water using two-color laser induced fluorescence," Exp. Fluids **26**(1–2), 7–15 (1999).
30. P. Reungpatthanaphong, S. Dechsupa, J. Meesungnoen, C. Loetchutinat, and S. Mankhetkorn, "Rhodamine B as a mitochondrial probe for measurement and monitoring of mitochondrial membrane potential in drug-sensitive and -resistant cells," J. Biochem. Biophys. Methods **57**(1), 1–16 (2003).
31. Y. Y. Chen and A. W. Wood, "Application of a temperature-dependent fluorescent dye (Rhodamine B) to the measurement of radiofrequency radiation-induced temperature changes in biological samples," Bioelectromagnetics **30**(7), 583–590 (2009).
32. S. Kohler, R. P. O'Connor, T. D. Thao Vu, P. Leveque, and D. Arnaud-Cormos, "Experimental microdosimetry techniques for biological cells exposed to nanosecond pulsed electric fields using microfluorimetry," IEEE Trans. Microw. Theory Tech. **61**(5), 2015–2022 (2013).
33. D. Arnaud-Cormos, P. Leveque, Y. H. Wu, J. M. Sanders, M. A. Gundersen, and P. T. Vernier, "Microchamber setup characterization for nanosecond pulsed electric field exposure," IEEE Trans. Biomed. Eng. **58**(6), 1656–1662 (2011).

1. Introduction

Near infrared laser light is used in many biological applications, including multiphoton microscopy [1], photodynamic therapy [2] and neural stimulation [3,4]. The exposure of biological tissues to infrared laser light poses a recurring question [5]: is the tissue health compromised due to the infrared exposure and does this transient hyperthermic stress cause any persistent damage to the cell? In the field of neural stimulation, this question concerns the mechanism of action and specifically whether it has a thermal effect acting on temperature sensitive ion channels [6] or a more direct effect on membrane capacitance due to the gradient of temperature [7]. One of the important challenges in understanding the effect of infrared exposure on biological tissues is the quantification of the local temperature in the exposed cells [8].

Similarly, nanosecond pulsed electric fields (nsPEFs) are an emerging tool with potential for both neurostimulation [9] and cancer treatment [10], depending on the intensity and pulse duration used. nsPEFs can be used to transiently permeabilize the plasma membranes of cells [11,12], but despite having high peak power, the effect of these ultrashort pulses are

#247362 Received 6 Aug 2015; revised 19 Sep 2015; accepted 22 Sep 2015; published 24 Sep 2015

considered to be nonthermal due to the low average energy density that they deliver. Interestingly, it has been shown analytically that the application of nsPEFs to cells could result in both thermal (Joule heating) and electrical effects [13]. Thus, like infrared laser light, local temperature measurements of biological samples exposed to nsPEFs are necessary to better understand the mechanisms involved in these effects.

A number of different microscopy techniques can be used to map temperature at the single-cell level to study thermal effects caused by infrared laser light or electrical sources [14] and each has its strengths and weaknesses. For example, Shang and colleagues [15] demonstrated the utility of fluorescence lifetime microscopy for cellular and subcellular measurements of temperature; however, this method is highly sensitive to pH and viscosity. Another highly promising technique is based on the anisotropy of fluorescence from green fluorescent protein [16], yet this requires the use of cell lines stably expressing fluorescent proteins, making it less suitable for studies of neurons or primary tissues that are difficult to transfect. A wide variety of other methods have been used, taking advantage of the temperature sensitivity of fluorescent quantum dots [17], Europium thenoyltrifluoroacetonate (EuTTA) [18], Er^{3+}-doped nanoparticles [19] or doped silica nanoparticles containing a combination of these substances [20]. The application of these techniques is limited by the toxicity of these substances and differential uptake and repartition in into organelles and membranes.

Rhodamine B (RhB) is a well-known water soluble fluorophore, with an absorption peak centered at 554 nm, and an emission peak at 576 nm. In the current context, the most interesting property of this molecule is its temperature dependent fluorescence quantum yield [21], which decreases linearly as temperature increases [22]. The fluorescence of RhB is negligibly pressure sensitive and pH independent above a pH of 6 [23]. RhB has been used in several microfluidic applications [24–29], and interestingly, distributes across biological membranes where it has been used as a mitochondrial probe [30]. These properties lead us to test whether RhB dye could be successfully used as optical thermometer in small biological compartments at the subcellular level. It has been used recently in the measurement of temperature in rat tail tendon samples exposed to radiofrequency electromagnetic fields [31], and similarly used in our group to measure temperature in cells exposed to continuous wave microwaves [32].

In this paper, we present experiments applying RhB to measure temperature at the cellular level to highlight the temperature changes induced in cells focally exposed to infrared laser light at 800 nm or 10 ns pulsed electric fields. First, the setup and the calibration procedure are detailed. Then, the different exposure systems are described that were used to deliver infrared laser light or nsPEFs to U87 human cancer cells during imaging experiments. The thermal effect of continuous infrared exposure was investigated, including the influence of the power of the radiation used and the distance between the source of infrared and the cells. The effects of an intermittent infrared exposure on the temperature of the cells was also investigated. Finally, the influence of nsPEFs on local cellular temperature was studied as a function of intensity, pulse number and repetition frequency. In the case of the exposure to nsPEFs, the temperature measurements made with RhB were compared with those completed with a calibrated external thermometer. In both cases, the local increase of temperature due to nsPEFs was demonstrated. RhB was therefore a highly sensitive and useful tool for investigating the cellular-level temperature impact of these stimuli.

2. Experimental setup

Figure 1(a) shows the experimental setup used for both infrared and nsPEFs exposure experiments that was located in a room with a stabilized temperature at 23°C. The setup can be divided into three parts, including the systems for imaging and measuring the temperature (lower part of the figure) and the systems for controlling and exposing cells to infrared laser light (upper right part of the figure) and to nsPEFs (upper left part of the figure). Figure 1(b) shows an expanded view of the petri dish when the nsPEFs delivery system was applied (left part of the figure) and when the infrared delivery system was used (right part of the figure).

#247362 Received 6 Aug 2015; revised 19 Sep 2015; accepted 22 Sep 2015; published 24 Sep 2015

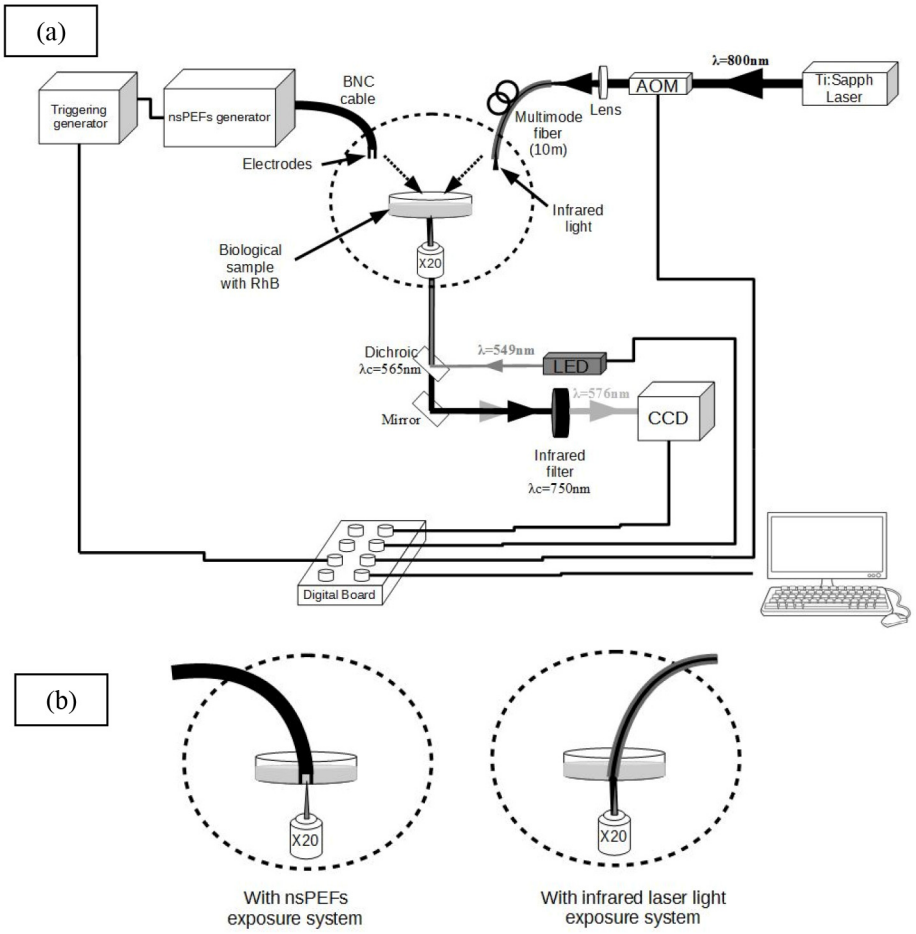

Fig. 1. (a). Experimental setup. (b) Zoom on the delivery of nsPEFs and infrared in the petri dish.

2.1. Rhodamine B fluorescence intensity measurement and conversion to temperature

The setup allowed the detection of the RhB fluorescence using wide field epifluorescence microscope (Leica DMI6000 B). The excitation light for RhB (λ = 549 nm) was provided by a light emitting diode (LED)-based light engine (Spectra7, Lumencor). This light, with an average power of 3.5 mW, was delivered to the cells with a dichroic mirror centered at 565 nm. A 20X objective was used to focus the light from the LED in the petri dish containing the cells loaded with RhB. The fluorescence emission (peak λ = 576 nm) of RhB was then collected through the dichroic mirror and separated from any infrared light with a longpass filter (λ_c = 750 nm) and detected with a electron-multiplying charge-coupled device camera (EM-CCD, 16 bit, pixel matrix 512x512, Evolve 512, Photometrics). All elements in the fluorescence imaging setup were controlled and synchronized by freely available software (Winfluor, Strathclyde University). The parameters of acquisition of the CCD was controlled as well as the LED engine by the software and by an analog output from digital acquisition (DAQ) board (USB-6229-BNC, National Instruments).

The calibration procedure was divided in two steps that occured simultaneously. Fig. 2 shows an example of the conversion of the fluorescence into temperature. For this calibration procedure, RhB was diluted in 2.5 mL of water in a petri dish to a final concentration of 50 µM. The petri dish was placed in a metallic ring containing a resistive element and

#247362 Received 6 Aug 2015; revised 19 Sep 2015; accepted 22 Sep 2015; published 24 Sep 2015

temperature controller (TC-E35, Bioscience Tools). The whole solution was heated from 23°C to 29°C by the heater element. At the same time, the evolution of the fluorescence intensity was recorded by the imaging software and was synchronized with the output voltage of the fiber thermometer. Fig. 2(a) shows an example of these results. A calibrated fiber optic thermometer (LUXTRON 812 Industrial Temperature Monitor) with an analog voltage output was used that allowed extraction of a linear relationship between the temperature of the sample (measured with the thermometer) and the voltage output of the fiber thermometer, as acquired by software. Fig. 2(b) shows a recording of the temperature over time. Finally, by extracting the previous results in time, it was possible to extract the relationship between the evolution of the fluorescence intensity and the change of temperature. This setup therefore allowed measurement of the evolution of fluorescence intensity with the temperature of the RhB. Ten calibration procedures were performed and the average decrease of fluorescence intensity with temperature was found to be linear and estimated at 1.63% +/–0.2 per Celsius degree.

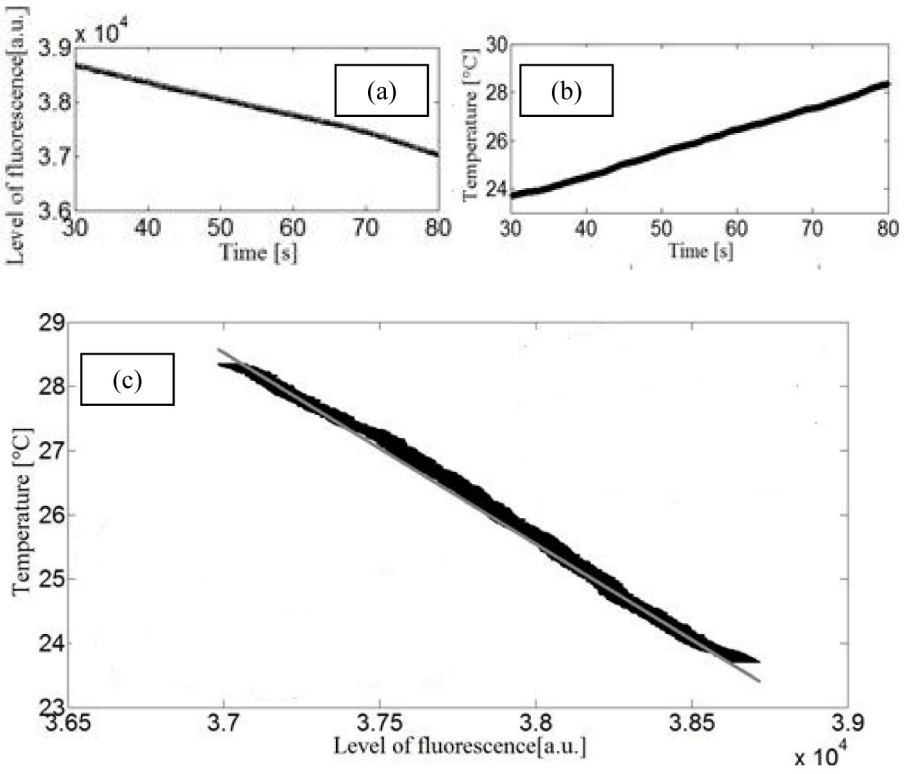

Fig. 2. (a). recording of the level of fluorescence versus time. (b). recording of the temperature with external thermometer versus time. (c). Conversion of fluorescence intensity into temperature. Results of measurement in black, linear fit in grey.

2.2. Shaping and routing of infrared laser light excitation

The infrared laser source was a femtosecond-pulsed tunable Titanium-Sapphire oscillator (Chameleon, Coherent, INC, 680-1080 nm, 10 nm, 140 fs, 4 W, 80 MHz). The central wavelength was fixed at 805 nm for all experiments. The laser beam was injected into a 10-m-long multimode graded-index fiber (GIF50C, Thorlabs). The fiber had a core diameter of 50 µm and a numerical aperture of 0.2, and caused a spectral broadening as presented in Fig. 3. The infrared laser light brought to the biological samples therefore had a spectral width of 19 nm at the full width half maximum (FWHM).

#247362 Received 6 Aug 2015; revised 19 Sep 2015; accepted 22 Sep 2015; published 24 Sep 2015

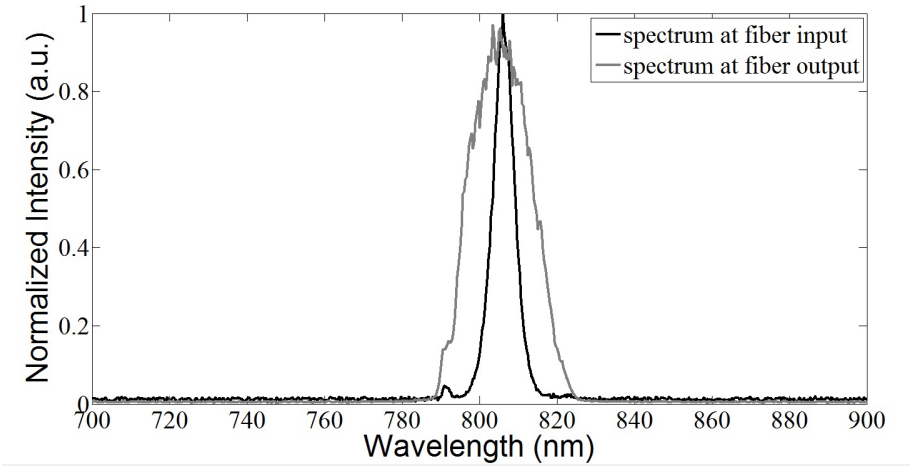

Fig. 3. Spectral broadening due to the fiber.

A maximum average power of 0.7 W was available at the fiber output, representing an injection efficiency of 78%. The infrared laser was rapidly modulated by an acousto-optical modulator (AOM, MT110IR, AA Optoelectronic), inserted before the fiber input. Transmission through the AOM was controlled by software and by the digital acquisition board allowing rapid and precise temporal control of infrared power to the biological samples. The switching delay between application of the voltage on the AOM and the response at the fiber output was measured to be 250 µs.

2.3. nsPEF delivery system

To study the impact of nsPEFs on local temperature, the nsPEF delivery system replaced the infrared delivery system (Fig. 1). The nanosecond pulse generator (FID Technology, 10 kV maximum voltage, 50 Ohm output impedance, 10 ns pulse width) was triggered by a function generator (Agilent 33120A) controlled by a custom Labview program (Labview 7.1, National Instruments). The trigger signal consisted of square pulses with a duty cycle of 10% and was recorded by the DAQ board during all experiments. The electric pulses delivered to electrodes by a high voltage cable. Bipolar electrodes were separated by a distance of 1.5 mm and connected in parallel to a 50 Ohm resistor to impedance-match the nsPEF generator, as previously described [33].

2.4. Preparation of U87 cell culture labelled with RhB

Human U87 glioblastoma cells were purchased from American Type Culture Collection (ATCC) and grown in Minimum Essential Media (MEM) supplemented with fetal bovine serum, glutamine and antibiotics and kept in an incubator under a 5% CO_2 atmosphere. Cells were detached with trypsin and subcultured onto glass bottomed petri dishes (Fluodish, WPI) and allowed to attach to glass in the incubator for 24 hours before experiments. Culture media was then removed from petri dishes containing adherent U87 cells, and replaced with a 50 µM RhB concentration made in a physiologically balanced HEPES buffered salt solution (HBSS) pH-buffered to 7.4. Cells were incubated with RhB for 2 hours to allow for dye incorporation. After the loading period, petri dishes were washed twice with fresh HBSS in order to remove extracellular dye and finally placed on the microscope stage.

3. Measurement of temperature of cells under infrared exposure

Figure 4 shows the image of the cells as detected by the CCD camera from the fluorescence of the RhB inside cells. It also shows an example of an area illuminated by the infrared laser from the optical fiber and an example of a region of interest (ROI) that was analyzed. Single cell ROIs were thus defined after positioning the infrared exposure area with a

#247362 Received 6 Aug 2015; revised 19 Sep 2015; accepted 22 Sep 2015; published 24 Sep 2015

micromanipulator. This ROI delimited the pixels that were considered in the recording of fluorescence intensity over time. The fluorescence intensity values of the pixels located in the ROI were averaged in order to extract the mean fluorescence intensity.

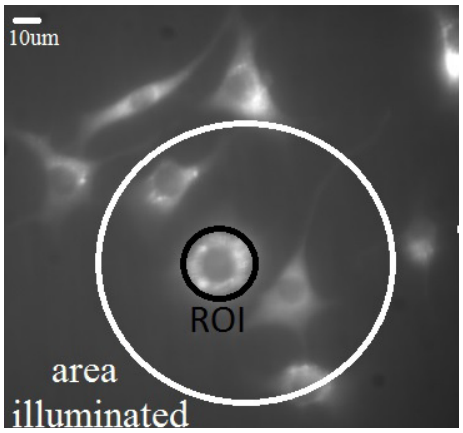

Fig. 4. Image of the cells labelled with RhB. Localisation of the infrared exposure area and definition of the region of interest where the cell temperature is measured.

3.1. Continuous infrared exposure

The first example of infrared laser exposure considered was a continuous application with a duration of 60 s and an average power at the fiber output of 200 mW (Fig. 5) . The optical fiber was placed 0.5 mm above the cells. The LED illumination occurred for a total duration of 200 s. High temporal resolution was not required in this case, so imaging was performed with temporal sampling of 200 ms in order to increase the signal to noise ratio. Infrared exposure induced an initial fast increase of temperature of 1.5 °C and eventually reached a steady state with the thermal balance between the contribution of energy by the infrared radiation and the thermal exchange with the extracellular bath. This steady state was observed when the temperature of the system stabilized and did not vary more than +/− 0.1 °C. After the end of the exposure, the temperature of the cell returned to its basal value (23 °C), demonstrating that the change in fluorescence of RhB with temperature was reversible. Experiments performed to examine the photobleaching of RhB by the LED illumination (data not shown) revealed an exponential term that could be approximated by a linear trend after 10 minutes, corresponding to a decrease of -2.10^{-3} °C/s. Before each experiments, we exposed the RhB to the LED illumination until we reached this linear decrease. All the following results were therefore corrected for this linear trend.

#247362 Received 6 Aug 2015; revised 19 Sep 2015; accepted 22 Sep 2015; published 24 Sep 2015

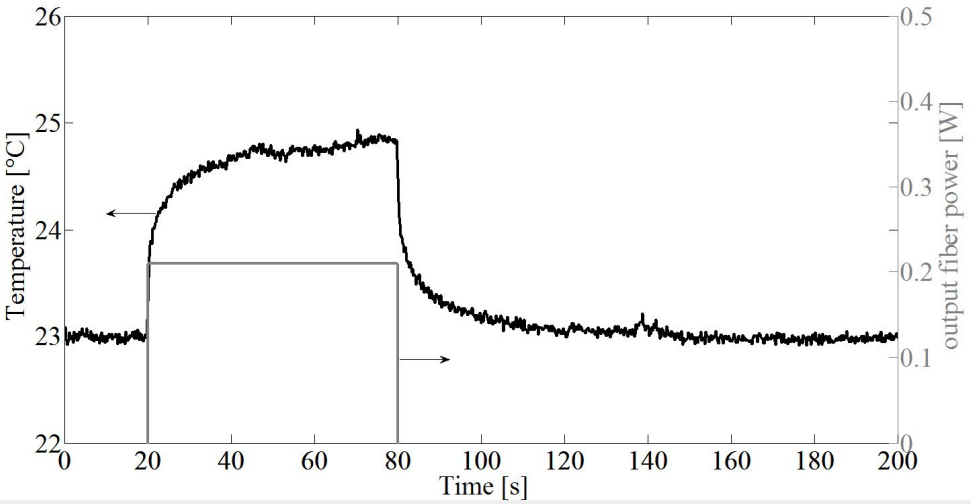

Fig. 5. Temperature measurement of cell under continuous infrared exposure.

3.2. Study of the impact of output fiber power

The impact of the average power at the output of the fiber on the temperature increase in cells was investigated. The average power at the output of the multimode fiber was varied from 100 mW to 700 mW by steps of 100 mW. The temporal resolution was set at 200 ms during a recording period of 200 s and the fiber output was positioned 0.5 mm above the cells. Fig. 6(a) presents the evolution of the temperature in the ROI. A linear dependence of the increase of temperature reached at the steady state with the infrared laser light power is highlighted in Fig. 6(b) . As expected, the temperature increase was higher with the use of infrared radiation with higher average power. Indeed, the change in temperature varied from nearly 0.5 °C at 100 mW) to nearly 5°C at 700 mW. The time constant, determined as the time when the temperature increase reached 63% of the final increase was found to be 2.4 s (+/−0.2 s) for all the power used as predicted by the linearity of the heat diffusion equation.

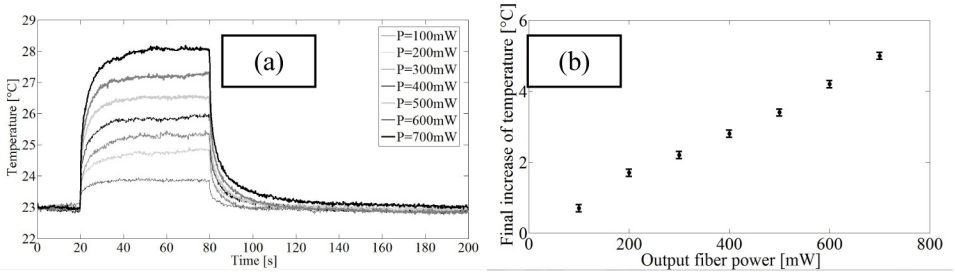

Fig. 6. (a). Evolution of temperature in cells depending on the average power P. (b). Evolution of the final increase of temperature depending on the average power at the output of the fiber with error bars illustrating the +/−0.1 °C of incertitude.

3.3. Intermittent pulsed infrared exposure

Intermitttent rectangular pulses of infrared exposure were used to evaluate the temporal resolution of the method. The average power at the output of the fiber was 500 mW and the fiber was maintained at a distance of 0.5 mm from the cells. The infrared exposure started after a baseline recording of 5 s and consisted of a series of 100 ms pulses modulated by the AOM each with a duration of 100 ms and delay of 50 ms (duty cycle = 67%) over a period of approximately 10 s. Fig. 7 presents the results. A magnified view of the temporal pattern of

#247362 Received 6 Aug 2015; revised 19 Sep 2015; accepted 22 Sep 2015; published 24 Sep 2015

the optical exposure is shown in the inset of Fig. 7 . The best temporal resolution that could be obtained was approximately 4 ms due to limitations in the camera readout and LED control speed. The intermittent infrared exposure induced a global increase of temperature of nearly 3.5 °C, from 23 °C to 26.5 °C. Furthermore, each pulse induced a small increase of temperature whereas the delay between pulses was associated with decrease of temperature not sufficient to return at the basal value. Unfortunately, the noise present in the measurement, due to the low integration time needed on the camera, prevented us to estimate obviously the value of the increase of temperature induced by one single pulse.

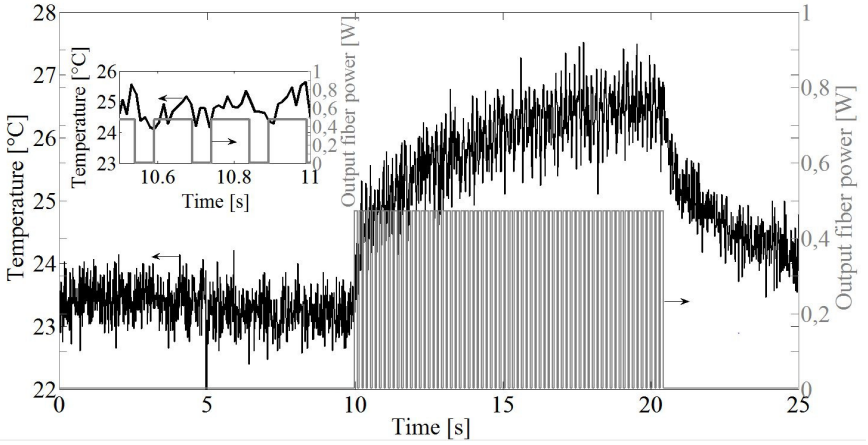

Fig. 7. Intermittent infrared exposure. Inset. Zoom from 10.5 s to 11 s.

4. Application of the optical measurement of temperature to cells exposed to nsPEFs

Given that RhB showed promise in measuring rapid temperature changes caused by infrared exposure, the method was used to study the impact of nsPEFs on local temperature at the cellular level. The bipolar electrodes were positioned with a micromanipulator so that the cells of interest were located in the field of view of the microscope and between the electrodes. ROIs were chosen selecting cells in the center of the field of view. In order to understand the contribution of pulse number and repetition frequency to potential heating at the cellular level, different pulse applications were tested from 1 single nsPEF to 100 nsPEFs with a frequency of 100 Hz including the configurations using 10 nsPEFs at 10 and 100 Hz and 100 at 10 Hz. Pulses were 10 ns long with an associated electric field between the electrodes of 44.1 kV/cm. The pulse trigger signal was recorded and synchronized with the measurement of RhB fluorescence using a temporal resolution of 200 ms so that the evolution of temperature with each pulse could be considered locally at the cellular level.

At the same time, temperature in the extracellular bath between the electrodes was measured and recorded with the fiber optic temperature sensor (Luxton). The Luxton fiber probe is a specialized temperature sensor that is immune to radiofrequency and high voltage interferences. These combination of the cellular measurement of temperature with RhB and the extracellular recordings with the Luxtron sensor allowed the comparison of their relative sensitivities to local temperature changes with time.

The results of these two techniques are shown in Fig. 8 . Table 1 summarizes the temperature changes as measured by RhB fluorescence and the Luxtron temperature probe.

#247362 Received 6 Aug 2015; revised 19 Sep 2015; accepted 22 Sep 2015; published 24 Sep 2015

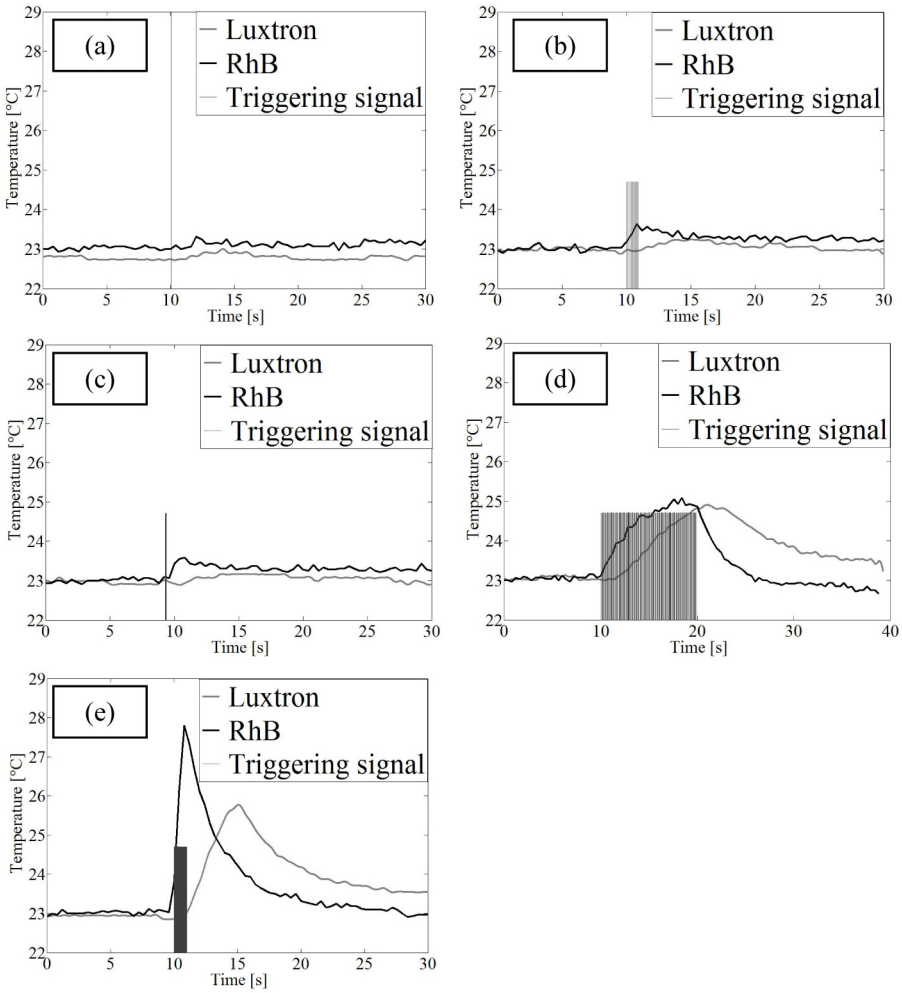

Fig. 8. Temperature modification induced by nsPEFs as simultaneously measured by RhB fluorescence and Luxtron thermometer. (a). 1 single pulse. (b). 10 nsPEFs at 10 Hz. (c). 10 nsPEFs at 100 Hz. (d). 100 nsPEFs at 10 Hz. (e). 100 nsPEFs at 100 Hz.

Table 1. Recapitulative of temperature increases for both techniques and all parameters used.

		Number of pulses					
		1		10		100	
		RhB	Luxtron	RhB	Luxtron	RhB	Luxtron
Frequency (Hz)	10	0°C	0°C	0.6°C	0.3°C	2.1°C	2°C
	100	0°C	0°C	0.6°C	0.3°C	4.8°C	2.8°C

No significant temperature changes were observed with the delivery of a single 10ns pulse with either the RhB measurement at the cellular level or the Luxtron probe between the electrodes (Fig. 8(a)) . With the application of 10 nsPEFs, for both 10 Hz and 100 Hz the temperature elevation was measured at 0.6°C with RhB fluorescence. The influence of pulse repetition is apparent in the application of 100 nsPEFs since at 10 Hz, an increase of 2.1°C was detected whilst 4.8°C was observed at 100 Hz. The increase of the number of pulses also

#247362 Received 6 Aug 2015; revised 19 Sep 2015; accepted 22 Sep 2015; published 24 Sep 2015

induced an increase of local temperature between the electrodes. After the application of nsPEFs ceased, the delay of temperature decrease was several seconds, in the same order as that observed for infrared exposure. This time corresponded to the time necessary for the thermal exchanges with the external medium as temperature of the system returned to equilibrium with room temperature.

Important differences were observed in the measurement of temperature with the Luxtron probe, in comparison to the RhB method, specifically there was a delay between the time when RhB showed temperature changes and when the Luxtron detected changes in the extracellular volume between the electrodes. The difference was observed in the slope of the temperature increase reported by these two methods. The difference in the elevation of temperature can be explained by the fact that with the application of 10 pulses, the modification of temperature was very small. The results therefore show that the RhB temperature measurement had a better temporal resolution and better sensitivity for reporting changes in temperature at the cellular level than the external temperature probe. This was confirmed in experiments using pulse applications of 100 nsPEFs. In this case where a pulse repetition frequency of 10 Hz was used, the delay of the Luxtron probe was very evident. However at low pulse repetition frequencies, the increase in temperature registered by the Luxtron probe was similar to that measured at the cellular level with RhB. At a pulse repetition frequency of 100 Hz, the temporal resolution of the Luxtron probe was not sufficient to measure the temperature elevation before its dissipation. The external thermometer did not therefore represent the rate of change in temperature as observed at the cellular level with RhB fluorescence.

The influence of the amplitude of the nsPEFs was also studied in order to understand at which level of electric field temperature increases are observed. In this case, the delivery of 100 pulses with a frequency of 10 Hz was chosen. The duration of the pulses is still 10 ns. Temperature measurements with RhB and Luxtron thermometer were performed in this configuration, since the magnitude of the temperature change detected was approximately the same for both methods. The amplitude of the pulse was varied from 5.5 kV/cm to 44 kV/cm including 11, 17, 22, and 34 kV/cm. The results are shown in Fig. 9 . Figure 9(h) shows the relationship between the increase of temperature and the amplitude of the nsPEFs with error bars illustrating the +/–0.1 °C standard deviation.

#247362 Received 6 Aug 2015; revised 19 Sep 2015; accepted 22 Sep 2015; published 24 Sep 2015

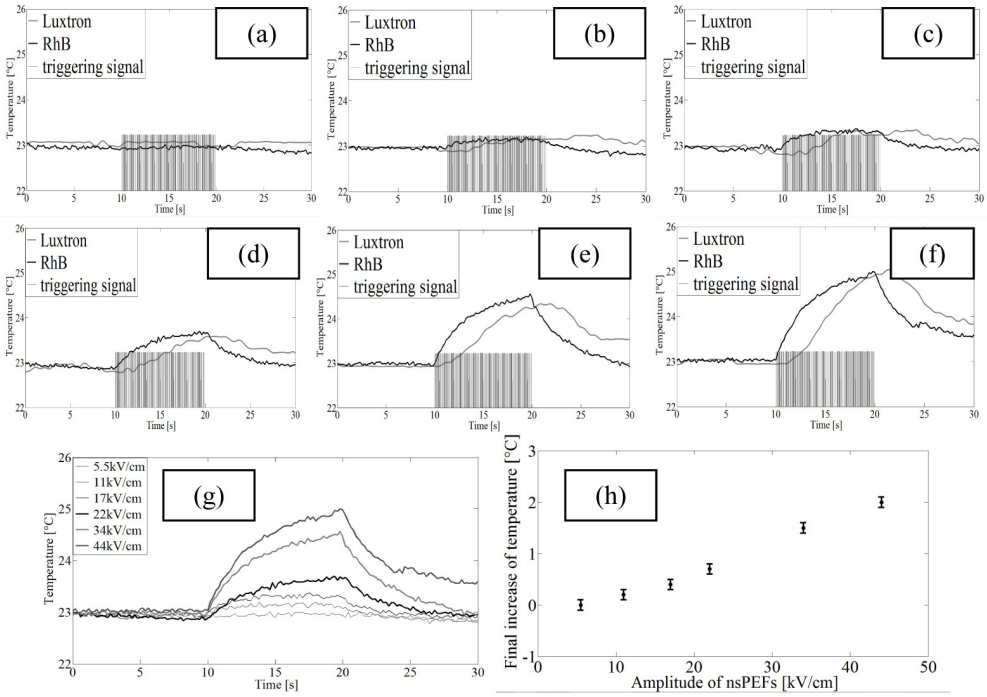

Fig. 9. The influence of pulse amplitude on temperature modifications induced by 100 x 10ns nsPEFs at 10 Hz, measured by RhB and Luxtron thermometer. (a). 5.5 kV/cm. (b). 11 kV/cm. (c). 17 kV/cm. (d). 22 kV/cm. (e). 34 kV/cm. (f). 44 kV/cm. (g). Superposition of RhB measurement curves. (h). The magnitude of the increase of temperature depending on the amplitude of the nsPEFs for an exposure to 100 pulses at 10 Hz.

The amplitude of the nsPEFs played a key role in the local increase of temperature induced by the pulse application. No increase of temperature was observable with the application of nsPEFs with an amplitude of 5.5 kV/cm with our thermal precision. At 11 kV/cm nsPEFs, a very small increase of temperature appeared of about 0.2 °C (+/–0.1°C) was detected. As one would expect, as pulse amplitude was increased, so did the change in temperature induced. Thus, with a fixed number of pulses at this frequency, the local increase of temperature was induced only if the amplitude of nsPEFs exceeded a certain threshold. With the thermal precision of +/–0.1°C accessible with our experiment, the threshold was therefore between 5.5 and 11 kV. This threshold would also be expected to decrease with longer pulse durations, however only pulses of 10 ns were considered in our experiments.

5. Conclusion

Among all the methods available for the microscopic measurement of temperature at the cellular level, RhB fluorescence is by far the simplest with respect to both the optical setup and ease of use for biologists. The temperature sensitivity of RhB, in particular the dependence of its quantum yield with regard to the temperature, has been used in many fluidic applications to make temperature measurement at the micron scale. In this paper, we developed a setup built around a wide field fluorescent microscope using epifluorescence detection to measure temperature in cells exposed to an infrared radiation at 805 nm and to nsPEFs. The thermal effect of each stimulus was demonstrated and it was shown that the increase of temperature induced depended on different parameters such as the average power, the duration of exposure the frequencies of repetition and their amplitude.

In these experiments, local temperature increases were demonstrated at the cellular level in samples exposed to 10 ns PEFs. The effect of nanosecond pulsed electric fields are assumed to be nonthermal, given their low average power and short duration. However, our

#247362 Received 6 Aug 2015; revised 19 Sep 2015; accepted 22 Sep 2015; published 24 Sep 2015

results suggest that temperature changes should be considered in their effects, particularly at higher electric fields, application frequencies and repetition rates.

This method is a first step in understanding some phenomena that are induced by heating biological tissues. The temporal resolution of the method was approximately 4 ms and the sensitivity allowed a detection of approximately 0.1°C change in temperature. This system now permits investigation of temperature modifications at the cellular level and can be combined with fluorescent physiological indicators that permit the measurement of intracellular calcium, plasma membrane potential and mitochondrial membrane potential. The method presented provides an excellent compromise between temporal resolution and sensitivity to measure the thermal impact of infrared radiation and nsPEFs at the cellular level to understand their mechanisms and advance their potential use in therapeutic applications.

Author Contributions

RO, DM and CL conceived of the experiments and wrote the manuscript. RO,CL and DM developed the infrared optical stimulation apparatus and RO, DM integrated it with the fluorescence imaging system. PL developed the nanosecond pulsed electric field application system performed FDTD simulations calculating the electric field. DM and RB performed temperature experiments with nsPEFs. DM, CL performed infrared heating experiments and analyzed data.

Acknowledgments

Research was funded through an ANR Labex Excellence Chair awarded to RO as part of Labex SigmaLim, funds from the Region Limousin and the CNRS. The BioEPIX laboratory at XLIM are part of the European Associated Laboratory (LEA) entitled “Pulsed Electric Fields Applications in Biology and Medicine”.

#247362 Received 6 Aug 2015; revised 19 Sep 2015; accepted 22 Sep 2015; published 24 Sep 2015